Powder Technology 354 (2019) 108–114

Contents lists available at ScienceDirect

Powder Technology

journal homepage: www.elsevier.com/locate/powtec

On the shear viscosity of dilute suspension containing elliptical porous particles at low Reynolds number

Jiajia Liu [a,b], Chenggong Li [a], Mao Ye [a,*], Zhongmin Liu [a]

[a] Dalian National Laboratory for Clean Energy, National Engineering Laboratory for MTO, Dalian Institute of Chemical Physics, Chinese Academy of Sciences, Dalian 116023, Liaoning, China
[b] University of Chinese Academy of Sciences, Beijing 100049, China

ARTICLE INFO

Article history:
Received 16 November 2018
Received in revised form 5 April 2019
Accepted 24 May 2019
Available online 31 May 2019

Keywords:
Elliptical porous particle
Relative viscosity
Intrinsic viscosity
Lattice Boltzmann model
Darcy number

ABSTRACT

In view of the significance of non-spherical and permeable particles in liquid-solid and gas-liquid-solid reactors in industrial processes, it is essential to understand and quantify the rheological properties of multiphase flows in these processes. In this study, we investigate the shear viscosity of dilute suspension containing elliptical porous particles at low Reynolds number *Re* of $O(0)$ by use of a modified lattice Boltzmann model. The fluid flow around and inside an elliptical porous particle is described by the volume-averaged macroscopic governing equations. The relative viscosity is calculated for an elliptical porous particle rotating in a two-dimensional (2D) simple shear flow, based on the relation between the shear stress and the second order moments of non-equilibrium particle distribution function. The effects of porous structure of the elliptical particle on the viscosity and flow field are investigated with different axis ratios in detail. Our results demonstrate that the relative viscosities of dilute suspension containing elliptical porous particles increase linearly with solid volume fraction at various Darcy number for particles with varying axis ratios. Moreover, a simple empirical expression for intrinsic viscosity is proposed as a function of Darcy number.

1. Introduction

Liquid-solid and gas-liquid-solid flows are frequently encountered in multiphase reactors in a wide variety of industrial processes. It is therefore essential to study the interaction between fluid and solids in these processes, which aim ultimately at the understanding of rheological properties that are critical for design and operation of liquid-solid and gas-liquid-solid reactors. Among the rheological properties of fluid flow, the viscosity, which is a measure of resistance to the friction between different fluid layers or between fluid flow and boundary walls, has attracted considerable interests for centuries. For example, over a century ago, Einstein studied the viscosity of dilute suspensions containing solid spheres and proposed the well-known Einstein's viscosity formula [1]. Despite its widespread applications, the Einstein's formula actually demonstrates that the macroscopic rheological properties of multiphase flow are closely related to the underlying physics at micro scale when hydrodynamic interaction is dominant. According to Einstein's formula, the relative viscosity of dilute suspensions containing solid spheres can be calculated via

$$\eta_r = \mu^*/\mu_f = 1 + [\eta]\phi \tag{1}$$

where μ^* is the viscosity of suspension, μ_f is the viscosity of pure fluid, ϕ is the solid volume fraction, $[\eta]$ is the intrinsic viscosity which is equal to 2.0 in 2D and 2.5 in 3D case [2], and η_r is the ratio of viscosity of suspension to that of pure fluid, i.e., the relative viscosity. However, the Einstein's viscosity formula, which is based on the non-interacting suspensions, can only be used for spherical particles at very low solid volume fraction, usually $\phi < 0.02$. This limits its applications in multiphase reactors as, in practical liquid-solid and gas-liquid-solid flows, solid volume fraction, particle shape and particle permeability will affect the viscosity.

Many studies considered the effect of particle shape on viscosity of suspensions. Jeffery extended the Einstein's viscosity formula to the suspension containing solid ellipsoidal particles at low *Re* where the effect of inertia can be neglected [3]. It has been shown that the viscosity can be similarly expressed as a formula as Einstein's but a revised factor which varies with the initial configurations needs to be incorporated. Yamamoto et al. studied numerically the effects of various factors on the intrinsic viscosity of dilute suspension of rodlike particles in a simple shear flow at low *Re*, such as orientation angle, rotation orbit and aspect ratio of particles [4]. Recently, Huang et al. studied the shear viscosity of suspension of prolate and oblate spheroids by lattice Boltzmann simulations for *Re* of $O(100)$. They found that both axis ratios of solid ellipsoids and *Re* affect the intrinsic viscosity significantly [5]. As for high solid volume fraction, Krieger and Thomas [6] developed a semi-empirical model for viscosity of suspension of randomly monodispersed hard

* Corresponding author.
E-mail address: maoye@dicp.ac.cn (M. Ye).

https://doi.org/10.1016/j.powtec.2019.05.068
0032-5910/

spherical particles with a maximum solid volume fraction ϕ_m. Mueller et al. [7] measured the rheology of suspensions of monodisperse particles of varying aspect ratios for solid volume fraction from dilute to highly concentrated by experiments, and the derived empirical relationships can be used to predict the rheology of suspensions of prolate particles well. There are also many different numerical methods adopted by researchers to calculate the viscosity of suspensions [8–10]. However, the effects of the particle shape and solid volume fraction on the viscosity of suspensions are only limited to the solid impermeable particles in above studies.

In practice, the porous and permeable particles are widely found in either industrial or natural processes [11,12]. The porous structure of these particles can affect the interaction between particles and fluid, and thus influence the rheological properties of the particle-fluid system [13]. Joseph and Tao carried out a theoretical analysis on the interactions between a porous particle and the viscous fluid, though at low *Re*, they found that the effect of permeability of a porous sphere on drag force is equivalent to the reduction of the radius of an impermeable sphere [14]. Bhattacharyya et al. applied a two-dimensional flow model to investigate the flow field and solute transport through and around a porous cylinder at *Re* of 1 to 40 [15]. It turned out that the drag force on the porous cylinder reduces monotonically with the increase of *Re* and decrease of *Da*. Shahsavari et al. [16] studied the steady viscous flow past and through a porous cylinder between two parallel plates by the commercial software COMOL Multiphysics 4.3a, and discussed the effect of *Da*, *Re* and blockage ratio on the flow pattern. Recently, the dynamics of porous particle in a simple shear flow was investigated by theoretical analysis and numerical simulation [13,17,18]. Their results revealed that the flow patterns inside and outside particles significantly depend on the permeability [13,17,18]. Even though the permeability has little effect on the rotation behavior of porous particle in Stokes flow regime [17], the role of permeability cannot be neglected as the increase of fluid inertia [18]. Later, Xu et al. investigated numerically the effects of permeability on shear viscosity of suspension of one porous spherical particle in shear flow at $Re \le 40$ [13]. Results showed that the intrinsic viscosity only depends on the Darcy number, and changes linearly as the increase of $\log(Da)$ at high Darcy number regime. However, the variation of intrinsic viscosity would be more complex for the suspension of elliptical or ellipsoidal particles [5], especially for the porous ones.

Therefore, we focus on the viscosity of suspension of an elliptical porous particle in a 2D simple shear flow at low Reynolds number. To describe fluid flows outside and inside moving porous particle, we adopt the volume-averaged macroscopic governing equations with the transient and nonlinear inertial term [19], which could be reduced to the Darcy's law and Brinkman equation under the Stokes flow conditions. A modified single relaxation time lattice Boltzmann model is used to numerically solve the corresponding macroscopic equations. The effects of the permeability and axis ratio of the elliptical porous particle are investigated in the shear flow. Our numerical results reveal that the relative viscosity of suspension changes linearly with solid volume fraction at various *Da* for different axis ratios of elliptical particle and the permeability can influence the intrinsic viscosity significantly.

2. Method

2.1. Governing equations

In this work, an elliptical porous particle rotating in a 2D simple shear flow is considered. The computational domain is set with a width of W and a height of $H = W/2$. The simple shear flow is driven by the two bounding walls moving in the opposite directions at constant velocity U with $Re = 0.08$. The Reynolds number is defined as $Re = \Gamma d^2/\nu$ where Γ is the shear rate with $\Gamma = 2U/H$. d is the characteristic length and ν is the kinematic viscosity of fluid. The volume-averaged macroscopic equation in terms of intrinsic phase average velocity, which can include the effects of fluid inertia [19], is used to describe the fluid flow around and inside the porous particle. The macroscopic equations are derived from microscopic equations averaged in a representative element volume (REV) scale which is much smaller than the particle and much larger than the size of pore structures.

$$\nabla\cdot\langle \boldsymbol{u}_f\rangle^f = 0 \tag{2}$$

$$\rho_f\left[\frac{\partial\langle \boldsymbol{u}_f\rangle^f}{\partial t} + \langle \boldsymbol{u}_f\rangle^f\cdot\nabla\langle \boldsymbol{u}_f\rangle^f\right] = -\nabla\langle p_f\rangle^f + \mu\nabla^2\langle \boldsymbol{u}_f\rangle^f + \boldsymbol{F}_m \tag{3}$$

where ρ_f is the fluid density, μ is the fluid viscosity, and $\langle \boldsymbol{u}_f\rangle^f$ and $\langle p_f\rangle^f$ are the intrinsic phase average velocity and pressure, respectively. Note that the subscript f refers to the fluid phase. The intrinsic average is defined by

$$\langle\psi_k\rangle^k = \frac{1}{V_k}\int_{V_k}\psi_k dV \tag{4}$$

where V_k and V denote the volume of k-phase and the volume of representative element, respectively. ψ_k refers to a quantity of k-phase. The total body force $\boldsymbol{F}_m$ in Eq. (3) can be calculated via

$$\boldsymbol{F}_m = -\frac{\varepsilon\mu}{K}\left(\langle \boldsymbol{u}_f\rangle^f - \boldsymbol{V}_p\right) - \rho_f\frac{\varepsilon^2\boldsymbol{F}_\varepsilon}{\sqrt{K}}\left(\langle \boldsymbol{u}_f\rangle^f - \boldsymbol{V}_p\right)\left|\langle \boldsymbol{u}_f\rangle^f - \boldsymbol{V}_p\right| + \rho_f\boldsymbol{G} \tag{5}$$

where ε stands for the porosity of the porous particle, K is the permeability of porous particle which can be further related to Darcy number, $Da = K/D^2$, where D presents the characteristic length of porous particle, V_p is the intrinsic phase average velocity of particle phase, F_ε stands for the geometric function calculated via $F_\varepsilon = 1.75/\sqrt{150\varepsilon^3}$. It should be noted here that the permeability and porosity are used to describe the porous structure inside particle. In our work, we correlate permeability K with porosity ε via $K = \varepsilon^3 d_p^2/[150(1-\varepsilon)^2]$, where d_p denotes the characteristic diameter of filling grains inside the porous particle, which takes the value of 100 μm, following references [15, 17]. The first and the second terms of the right side of Eq. (5) present the linear and nonlinear drags due to the presence of porous media, and the last term $\rho_f\boldsymbol{G}$ is the external body force. Through adjusting the value of permeability, the governing equations can formulate both the porous region and pure fluid outside. Therefore, it does not require any explicit boundary condition at the interface between fluid and porous region.

2.2. Numerical method

A modified lattice Boltzmann model is used to solve the volume-averaged macroscopic equations because of its easy implementation, accuracy and natural parallelism for simulating complex particle two-phase flows [20–22]. For simplicity, the intrinsic phase average velocity of fluid phase $\langle \boldsymbol{u}_f\rangle^f$ is denoted by $\boldsymbol{u}$. Therefore, the lattice Boltzmann evolution equations can be written as

$$f_\alpha(\boldsymbol{x}+\boldsymbol{e}_\alpha\delta_t, t+\delta_t) - f_\alpha(\boldsymbol{x},t) = -\frac{1}{\tau}\left[f_\alpha(\boldsymbol{x},t) - f_\alpha^{eq}(\boldsymbol{x},t)\right] + \delta_t F_\alpha(\boldsymbol{x},t) \tag{6}$$

where $f_\alpha(\boldsymbol{x},t)$ and $f_\alpha^{eq}(\boldsymbol{x},t)$ are, respectively, the particle density distribution function and the equilibrium distribution function at position $\boldsymbol{x}$ for time t. Here, $\boldsymbol{e}_\alpha$ is the velocity configuration in α direction, τ is the relaxation time, and δ_t is the time step which usually is set to be one. The D2Q9 model is used in Eq. (6), and the equilibrium distribution function f_α^{eq} and the force term F_α are given by

$$f_\alpha^{eq}(\boldsymbol{x},t) = \rho_f\omega_\alpha\left[1 + \frac{\boldsymbol{e}_\alpha.\boldsymbol{u}}{c_s^2} + \frac{(\boldsymbol{e}_\alpha.\boldsymbol{u})^2}{2c_s^4} - \frac{\boldsymbol{u}^2}{2c_s^2}\right] \tag{7}$$

$$F_\alpha = \rho_f\omega_\alpha\left(1-\frac{1}{2\tau}\right)\left[\frac{\boldsymbol{e}_\alpha.F_m}{c_s^2} + \frac{\boldsymbol{e}_\alpha.\boldsymbol{u}}{c_s^4}(\boldsymbol{e}_\alpha.\boldsymbol{F}_m) - \frac{\boldsymbol{u}.\boldsymbol{F}_m}{c_s^2}\right] \tag{8}$$

where ω_α refers to the weight parameter, i.e., $\omega_0 = \frac{4}{9}$ $\omega_{1-4} = \frac{1}{9}$ and $\omega_{5-8} = 1/36$. The macroscopic properties are calculated via

$$\rho = \sum_{\alpha=0}^{8} e_\alpha f_\alpha \tag{9}$$

$$\rho \boldsymbol{u} = \sum_{\alpha=0}^{8} e_\alpha f_\alpha + \frac{1}{2}\delta_t \rho \boldsymbol{F}_m \tag{10}$$

Owing to the equation's quadratic nature, $\boldsymbol{u}$ can be given by [23].

$$\boldsymbol{u} = \frac{\boldsymbol{v}}{d_0 + \sqrt{d_0^2 + d_1 \mid \boldsymbol{v} \mid}} + \boldsymbol{V}_p \tag{11}$$

where $\boldsymbol{v}$ is the temporal variable, which is defined as

$$\rho \boldsymbol{v} = \sum_{\alpha=\boldsymbol{0}}^{\boldsymbol{8}} \boldsymbol{e}_\alpha f_\alpha + \frac{\boldsymbol{1}}{\boldsymbol{2}}\delta_t \rho \boldsymbol{G} - \rho \boldsymbol{V}_p \tag{12}$$

The two parameters d_0 and d_1 can be calculated via

$$d_0 = \frac{1}{2}\left(1 + \frac{1}{2}\delta_t \frac{\varepsilon v}{K}\right) \tag{13}$$

$$d_1 = \frac{1}{2}\delta_t \frac{\varepsilon^2 F_\delta}{\sqrt{K}} \tag{14}$$

2.3. The interaction between particle and fluid

To compute the motion of particle in the fluid, the Newton equations and Euler equations are adopted to describe the translational and rotational behavior, respectively. The hydrodynamic drag force exerted on particles by surrounding fluid can be calculated via both the stress integration method [24] and momentum-exchange method [25]. It is shown that the momentum-exchange method is reliable, accurate, and easy for implementation in terms of drag force calculation. Thus in this work the momentum-exchange method is used as in Ref. [25].

The drag force $\boldsymbol{F}$ exerted on solid body by fluid can be expressed as

$$\boldsymbol{F} = \sum_{all\ x_b} \sum_{\alpha \neq 0} \boldsymbol{e}_\alpha \left[\tilde{f}_\alpha(\boldsymbol{x}_b, t) + \tilde{f}_{\overline{\alpha}}(\boldsymbol{x}_b + \boldsymbol{e}_{\overline{\alpha}}\delta_t, t)\right] \times [1 - w(\boldsymbol{x}_b + \boldsymbol{e}_{\overline{\alpha}}\delta_t)] \tag{15}$$

where $\boldsymbol{x}_b$ is the position of boundary node inside the solid particle, α is the direction from fluid node to boundary node, and $\overline{\alpha}$ is the direction opposite to α. $w(i,j)$ is a scalar array the value of which is set to be 0 when the lattice node (i,j) is occupied by fluid, and 1 when the lattice sites are inside the solid particle. Correspondingly, the torque acting on particle can be obtained by

$$\boldsymbol{T}_p = (\boldsymbol{x}_b - R) \times \boldsymbol{F} \tag{16}$$

where R is the mass center of the particle.

3. Model validation

In this section, our model is first validated by three cases: the free rotation of an elliptical particle in a simple shear flow, the simple shear flow around a fixed elliptical porous particle, and the shear viscosity of suspension of a freely rotating circular particle. In the simulations, we consider a neutrally buoyant porous particle, which means the particle density is set the same as fluid density.

3.1. The rotation of an elliptical particle in a simple shear flow

In this case, we simulate an elliptical particle freely rotating in a 2D simple shear flow at $Re = 0.08$ and $Da = 10^{-12}$. When the Darcy number is set to be significantly small ($Da = 10^{-12}$), the porous particle can be approximately treated as a solid particle. The elliptical particle with the major axis of $2a$ and minor axis of $2b$ is located in the center of the flow field with $H = 20a$. In this test case, we assume $a = 2b$. The characteristic length for elliptical particle is set to be $2a$ as in Ref [26]. We first check the grid independence by considering major axis $2a = 32$, 48, 64 lattice sizes. The angular velocity oscillates dramatically at some time steps when the major axis is resolved by 32 lattices. When the major axes are resolved by 48 and 64 lattices, the relative errors of computed angular velocities in both cases are within 0.5% and agree well with the analytical results by Jeffery. For saving computing resources and time, we finally choose the major axis resolved by 48 lattices in this test. Periodic boundary conditions are adopted to formulate the boundaries of fluid flow, and non-equilibrium bounce-back schemes [27] are used to describe boundaries in the bounding wall directions.

Jeffery developed an analytical solution for a solid elliptical particle freely rotating in a simple shear flow. The analytical expressions for the angle (orientation) and angular velocity of during the rotation are given by

$$\chi = tan^{-1}\left(\frac{a}{b}\ tan\frac{ab\Gamma t}{a^2 + b^2}\right) \tag{17}$$

$$\dot{\chi} = \frac{\Gamma}{a^2 + b^2}\left(a^2\ cos^2\chi + b^2\ sin^2\chi\right) \tag{18}$$

respectively. Fig. 1 shows the angle χ normalized by π racian and angular velocity $\dot{\chi}$ normalized by shear rate Γ of the elliptical particle at $Re = 0.08$. As can be seen from Fig. 1, the angular velocity $\dot{\chi}$ of the elliptical particle changes periodically with time which is normalized by the shear rate Γ, and the angle χ increases monotonously. It is demonstrated that our results for $Re = 0.08$ agree well with Jeffery's analytical results [3], which means our model is capable of capturing the accurate angular velocity and angle of rotating particle in a simple shear flow.

3.2. Torque on a fixed elliptical porous particle in a simple shear flow

In this second test case, we further investigate the simple shear flow around a fixed elliptical porous particle. The analytical solution of the torque exerted on an elliptical porous particle is given by Masoud et al. [17]

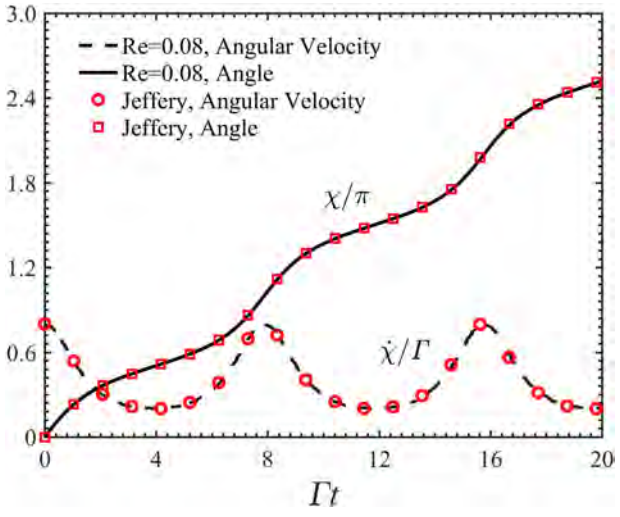

Fig. 1. Angle and angular velocity of rotation of the elliptical particle at $Re = 0.08$ and $Da = 10^{-12}$ as a function of dimensionless time Γt.

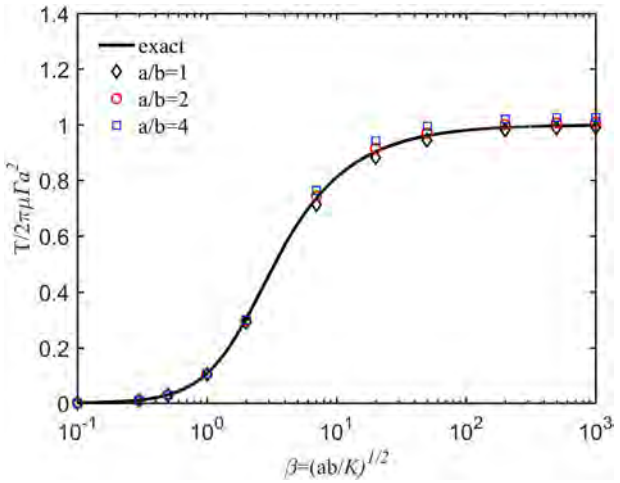

Fig. 2. Dimensionless torque as a function of dimensionless permeability for a fixed ellipse of various axis ratios.

$$T = 2\pi\mu\Gamma b^2 \frac{I_2(\beta)}{I_0(\beta)} \tag{19}$$

and β is calculated by

$$\beta = \sqrt{ab/K} \tag{20}$$

where I_2 and I_0 are the modified Bessel function. Fig. 2 shows the torque normalized by $2\pi\mu\Gamma a^2$ as a function of the permeability normalized by $a \times b$ for the fixed elliptical porous particle with different axis ratios. As can be seen, the simulated torque of the fixed porous particle well catches the analytical results. For $a/b = 1$, i.e. one circular particle, the maximum deviation appears at $\beta = 7$ with the relative error of 2.99%. As for the elliptical porous particles, the maximum deviation is about 4.28% for $a/b = 4$ at $\beta = 20$ and 1.51% for $a/b = 2$ at $\beta = 2$. The deviations can be considered as the numerical errors and are acceptable in terms of modelling validation. In this case, the implementation of permeability has been validated.

3.3. Shear viscosity of the suspension of a circular porous particle

We also obtained the shear viscosity of suspension of a single circular particle freely rotating in a simple shear flow at $Re = 0.08$ and

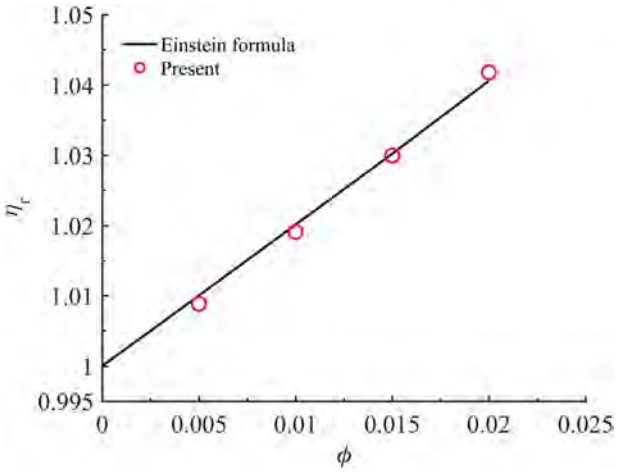

Fig. 3. The relative viscosity of suspension of a circular porous particle at $Re = 0.08$ and $Da = 10^{-12}$ as a function of solid volume fraction.

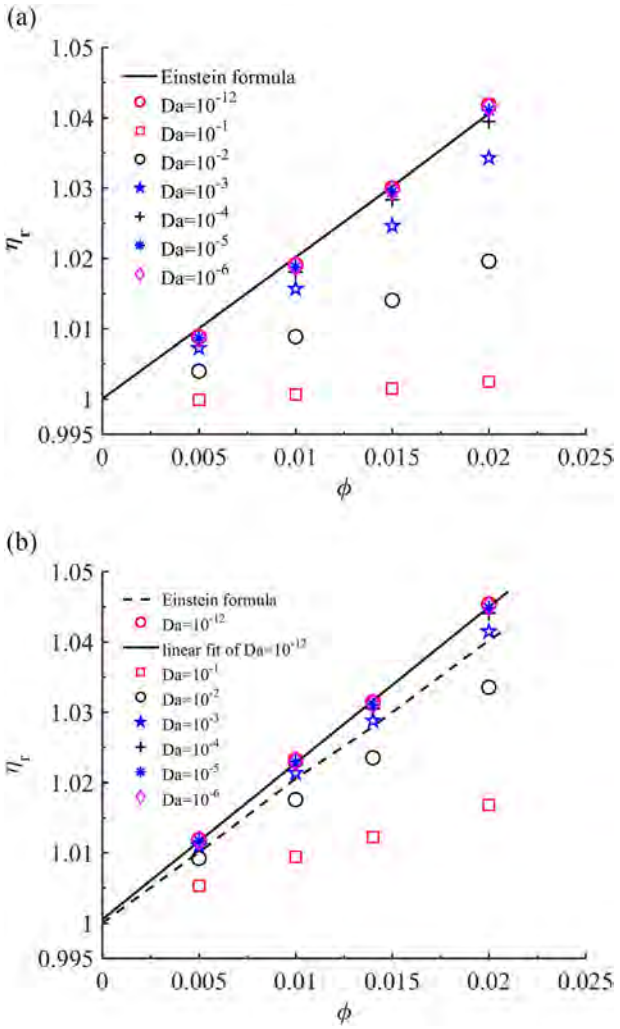

Fig. 4. The relative viscosity of suspension of an elliptical porous particle of (*a*) $A = 1$ and (b) $A = 2$ at various *Da*.

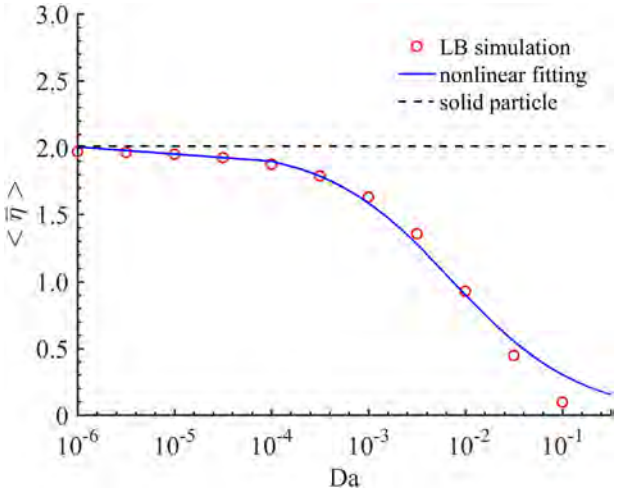

Fig. 5. The intrinsic viscosity of suspension of elliptical porous particle of axis ratio $A = 1$ as a function of *Da*.

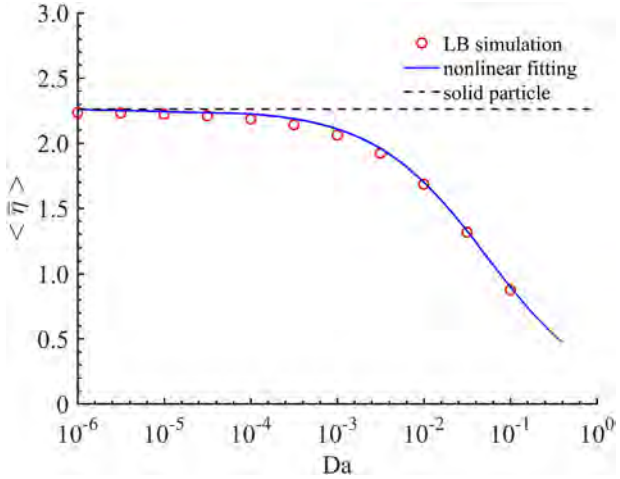

Fig. 6. The intrinsic viscosity of suspension of elliptical porous particle of axis ratio $A = 2$ as a function of Da.

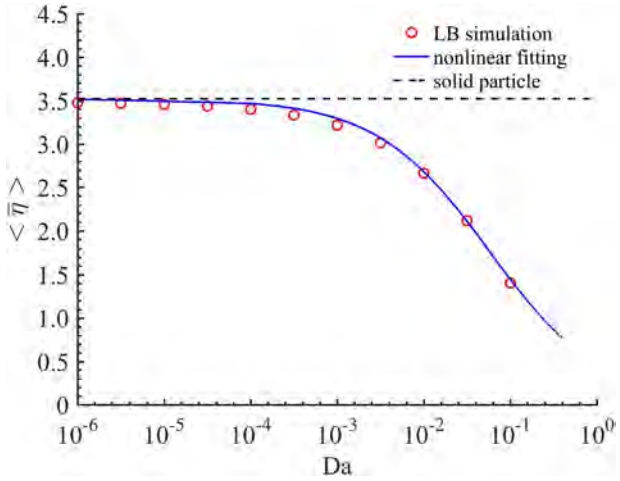

Fig. 7. The intrinsic viscosity of suspension of elliptical porous particle of axis ratio $A = 4$ as a function of Da.

Table 1
The intrinsic viscosity of elliptical porous particles with different axis ratios for various Da.

Da	Intrinsic viscosity of $a/b = 1$	Intrinsic viscosity of $a/b = 2$	Intrinsic viscosity of $a/b = 4$
1.0000×10^{-01}	0.0974	0.876	1.40
3.1623×10^{-02}	0.447	1.31	2.12
1.0000×10^{-02}	0.929	1.68	2.66
3.1623×10^{-03}	1.35	1.92	3.01
1.0000×10^{-03}	1.63	2.06	3.22
3.1623×10^{-04}	1.79	2.14	3.33
1.0000×10^{-04}	1.88	2.18	3.40
3.1623×10^{-05}	1.92	2.21	3.44
1.0000×10^{-05}	1.95	2.22	3.46
3.1623×10^{-06}	1.96	2.23	3.47
1.0000×10^{-06}	1.97	2.23	3.48

Table 2
The fitting parameters for correlation in Eq. 23

Parameters	Intrinsic viscosity of $a/b = 1$	Intrinsic viscosity of $a/b = 2$	Intrinsic viscosity of $a/b = 4$
m	2.01	2.26	3.54
n	27.6	7.47	7.16

$Da = 10^{-12}$. The relative viscosity can be calculated via

$$\eta_r = \frac{\nu_s}{\nu_f} = \frac{<\overline{\sigma}>}{\rho \nu_f \Gamma} \tag{21}$$

where $<\overline{\sigma}>$ refers to the time and space averaged shear stress [5]. The shear stress could be calculated by the second-order moments of non-equilibrium particle distribution functions,

$$\sigma(\mathbf{x}) = -\left(1 - \frac{1}{2\tau}\right) \sum f_\alpha^{neq} \boldsymbol{e}_{\alpha x} \boldsymbol{e}_{\alpha y} \tag{22}$$

where $f_\alpha^{neq} = f_\alpha - f_\alpha^{eq}$ stands for the non-equilibrium particle distribution function, and $\boldsymbol{e}_{\alpha x}$ and $\boldsymbol{e}_{\alpha y}$ refer to the x- and y-component of $\boldsymbol{e}_\alpha$, respectively. The particle diameter D is resolved by 40 lattices. The solid volume fraction is controlled by changing the scale of the flow field. As shown in Fig. 3, the relative viscosity increases linearly with the increase of solid volume fraction, which is consistent with the Einstein's formula, i.e. $\eta_r = \mu^*/\mu_f = 1 + 2.0\phi$. The consistency validates our model in simulating the shear viscosity of suspensions.

4. Results and discussion

In this section, we study the free rotation of a neutrally buoyant elliptical porous particle in a 2D simple shear flow. The effects of permeability on the shear viscosity of suspension are investigated with three different axis ratios, i.e. $A = a/b = 1, 2$ and 4. All the simulations are carried out with the minor axis resolved by 36 lattices after grid independence verification.

For comparison, Fig. 4(a) and (b) show the relative viscosities of suspensions of the elliptical porous particle with axis ratios $A = 1$ and 2, respectively. The shear viscosities are measured based on Eqs. (21) and (22) for the elliptical porous particle freely rotating in a simple shear flow. As shown in Fig. 4(a), the relative viscosity η_r of the suspension of one circular porous particle increases linearly with the solid volume fraction ϕ at various Da ranging from 10^{-12} to 10^{-1}. When Da is equal to 10^{-12}, the particle approaches to one solid particle, the relation between relative viscosity and solid volume fraction can be well fitted as $\eta_r = 1.0 + 2.0\phi$, which is in good agreement with Einstein's formula in 2D case. As the axis ratio increases to $A = 2$, as can be seen from Fig. 4(b), the relative viscosity is still a perfect linear function of the solid volume fraction for $Da = 10^{-12}$, which can be fitted as $\eta_r = 1.0 + 2.3\phi$ with the square of correlation coefficient of 0.9998.

The slope of the linear fitting function denotes to what extent the relative viscosity varies with the solid volume fraction. In this work the slope is named as intrinsic viscosity following some recent literature [4–6,13,17]. From our simulation results, the intrinsic viscosities of suspensions of elliptical porous particles of axis ratios $A = 1$ and 2, and 4 are 2.0, 2.3, and 3.5 for $Da = 10^{-12}$, respectively. The differences between these intrinsic viscosities are caused by particle ellipticity, which can be further explained by the flow patterns. In fact, the results of Jeffery et al. [3] and Huang et al. [5] confirmed that the intrinsic viscosity for suspension of an elliptical solid particle rotating in a simple shear flow changes with the ellipticity (i.e. $(a - b)/a$) of particles. As can be observed, both the results from our simulations and literature show that the intrinsic viscosity changes with the ellipticity of particles monotonously. Fig. 4 also shows that with the increase of Da, the slopes of the functions between the relative viscosity and solid volume fraction

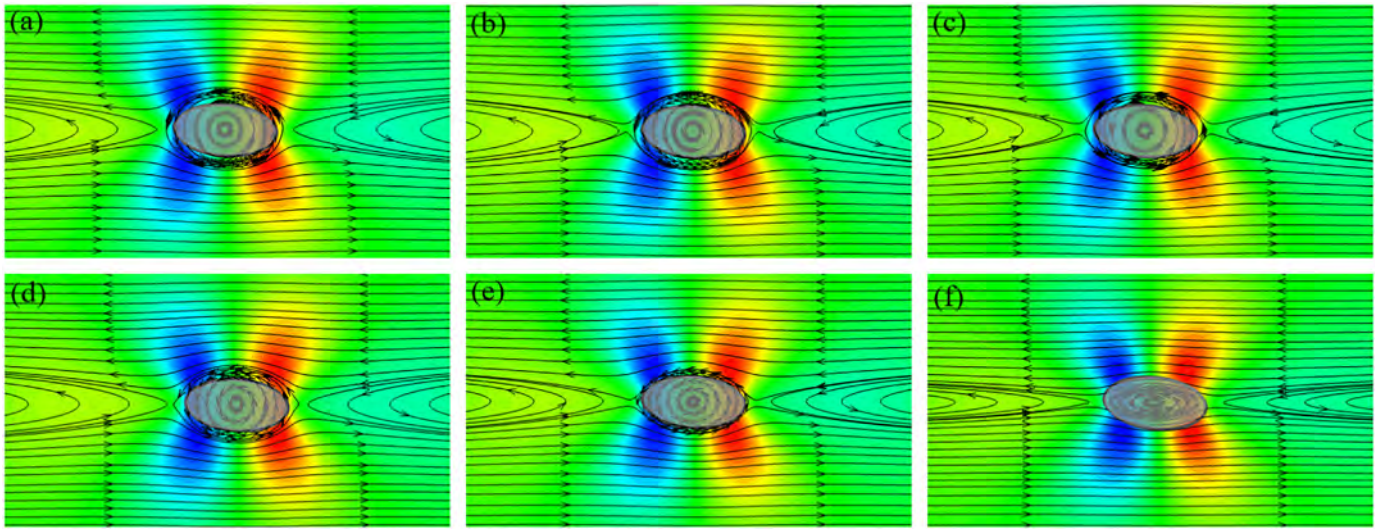

Fig. 8. Streamlines and vertical velocity contours for simple shear flows past a freely rotating elliptical porous particle for the same orientation at various *Da*: (a) $Da=10^{-6}$; (b) $Da=10^{-5}$; (c) $Da=10^{-4}$; (d) $Da=10^{-3}$; (e) $Da=10^{-2}$; (f) $Da=10^{-1}$.

decrease. For each *Da*, the relative viscosity increases monotonously with the solid volume fraction and there is a good linear relationship between them. Furthermore, the intrinsic viscosity for elliptical porous particle of axis ratio $A = 2$ is larger than that of circular particle at corresponding *Da*. This may also be caused by particle ellipticity.

The intrinsic viscosities of suspensions of an elliptical porous particle as a function of *Da* for three different axis ratios are shown in Figs. 5–7. Results reveal that the intrinsic viscosities decrease monotonously with the increase of *Da*. In this work, based on the data shown in Figs. 5–7, we propose a simple formula to correlate the intrinsic viscosity with the Darcy number

$$\langle\bar{\eta}\rangle = \frac{m}{1 + n \times Da^{2/3}} \tag{23}$$

where *m* is the intrinsic viscosity of suspension of the elliptical solid particle and the value of which can be obtained by LBM simulations of intrinsic viscosity of suspensions containing elliptical solid particles. The parameter *n* is a fitting constant which will change for different axis ratios *A*. The values of *m* are 2.01, 2.26 and 3.54 for elliptical solid particles of axis ratios $A = 1$, 2 and 4, respectively. Through fitting with least square method, the values of *n* take the values of 25.69, 6.90 and 6.54 for the elliptical porous particle of axis ratios $A = 1$, 2 and 4, respectively. We stress that the proposed formula of the intrinsic viscosity can work well for suspensions containing porous elliptical particles with the axis ratios of 1 to 4. For axis ratio beyond this range, it should be used with caution. Table 1 lists the intrinsic viscosities of elliptical porous particle with three different axis ratios for various *Da* and Table 2 summarizes the fitting parameters of Eq. (23).

We also plot streamlines and vertical velocity contours of *Da* ranging from 10^{-6} to 10^{-1} for the elliptical porous particle of axis ratio $= 2$ freely rotating in a simple shear flow at the same orientation in Fig. 8. It is argued that, for a solid elliptical particle, the shear layer close to the bounding walls moving in the opposite directions exerts a positive torque on the particle which is in favour of particle rotation, and the recirculation region in the middle of the channel exerts a negative torque which resists the rotation of this particle [28]. Besides, there is a third fluid layer near and around the particle surface that transfers momentum from moving bounding walls and recirculation region to the particle. However, for a porous particle, there are some streamlines that would penetrate and pass through the particle. As can be seen in Fig. 8 (a)-(f), with the increase of *Da*, there are more streamlines passing through the elliptical porous particle which means more fluid can penetrate through the porous media. And the flow patterns are similar to the simple shear flow past an impermeable elliptical particle in Ref. [28]. Furthermore, it is also demonstrated in Fig. 8 that, the larger the *Da*, the smaller the recirculation region of the flow. This in turn leads to a reduced negative torque exerted by the recirculation region on the porous particle. Therefore, the dynamic behaviors of the particle are different with various *Da* and the intrinsic viscosity will change accordingly.

Finally, the streamlines and vertical velocity contours for the elliptical particle with different axis ratios at $Da = 10^{-1}$ are presented in Fig. 9. The rotations of particles at the three cases are at steady state. For comparison, the particles in these three cases are at the same orientation angle. Results demonstrate that with the increase of axis ratios, the recirculation region of fluid flow is getting larger. The negative torque exerted by recirculation fluid on the particles may be influenced [18], and thus the interaction between elliptical particles and fluid differ

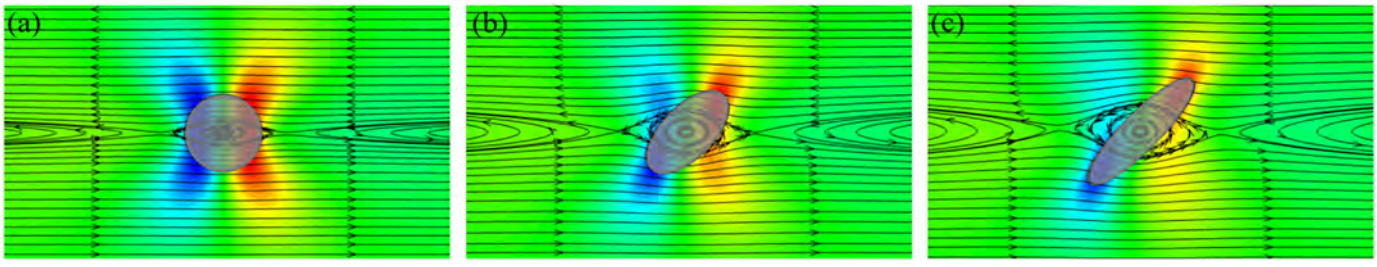

Fig. 9. Streamlines and vertical velocity contours for simple shear flows past a freely rotating elliptical porous particle at $Da=10^{-1}$ with different axis rations *A*: (a) $A = 1$; (b) $A = 2$; (c) $A = 4$.

in these three cases. Therefore, the rheological properties of the systems, for example, intrinsic viscosity, change.

5. Conclusions

In this work, we adopt a modified lattice Boltzmann model to solve the volume average macroscopic equations to simulate the rotation of one elliptical porous particle in the shear flow. The shear viscosity of this porous particle-fluid system is calculated by the non-equilibrium particle distribution functions. Firstly, we validate the lattice Boltzmann model by simulating an elliptical particle freely rotating in a simple shear flow, the torque acting on a fixed elliptical porous particle and the viscosity of suspension of a solid circular particle rotating in a simple shear flow. All the results agree well with the analytical solutions and the available results in the literature. Then, we mainly study the effects of permeability on the shear viscosity of suspension of an elliptical porous particle with different axis ratios. Our results confirm that Einstein's viscosity formula is only applicable to particles of solid circular particles. As for suspension of elliptical porous particle, the relative viscosity increases linearly with the solid volume fraction at various *Da*. As for intrinsic viscosity of suspension of elliptical porous particles of different axis ratios, we propose a general simple formula. Our results also demonstrate that more fluid can penetrate porous particle when *Da* is higher. The recirculation fluid regions increase with the axis ratios, and the change of intrinsic viscosity may be caused by recirculation fluid flow.

Acknowledgement

This work is subsidized by the National Natural Science Foundation of China (Grant no. 91834302).

References

[1] A. Einstein, Investigations on the theory of Brownian movement (Dover, New York, 1975), Ann. Phys. 34 (1911) 591.
[2] J.F. Brady, The Einstein viscosity correction in n dimensions, Int. J. Multiphase Flow 10 (1984) 113–114.
[3] G.B. Jeffery, The motion of ellipsoidal particles immersed in a viscous fluid, Proc. R. Soc. Lond. Ser. A 102 (1922) 161–179.
[4] S. Yamamoto, T. Matsuoka, Viscosity of dilute suspensions of rodlike particles: a numerical simulation method, J. Chem. Phys. 100 (1994) 3317–3324.
[5] H.B. Huang, Y.F. Wu, X.Y. Lu, Shear viscosity of dilute suspensions of ellipsoidal particles with a lattice Boltzmann method, Phys. Rev. E 86 (2012) 046305–1-0.6305-9.
[6] I.M. Krieger, J.D. Thomas, A mechanism for non-Newtonian flow in suspensions of rigid spheres, Trans. Soc. Rheol. 3 (1957) 137–152.
[7] S. Mueller, E.W. Llewellin, H.M. Mader, The rheology of suspensions of solid particles, Phys. Eng. Sci. 466 (2009) 1201–1228.
[8] S.V. Lishchuk, I. Halliday, C.M. Care, Shear viscosity of bulk suspensions at low Reynolds number with the three-dimensional lattice Boltzmann method, Phys. Rev. E 74 (2006) 017701–1-017701-4.
[9] Y.C. Yoshida, T.C. Katsumoto, et al., Prediction of viscosity of slurry suspended fine particles using coupled DEM-DNS simulation, Chem. Eng. Trans. 32 (2013) 2089–2094.
[10] V.A. Kuzkin, A.M. Krivtsov, A.M. Linkov, Computer simulation of effective viscosity of fluid-proppant mixture used in hydraulic fracturing, J. Min. Sci. 50 (2014) 1–9.
[11] P. Tian, Y.X. Wei, M. Ye, Z.M. Liu, Methanol to olefins (MTO): from fundamentals to commercialization, ACS Catal. 5 (2015) 1922–1938.
[12] H. Li, M. Ye, Z.M. Liu, A multi-region model for reaction–diffusion process within a porous catalyst pellet, Chem. Eng. Sci. 147 (2016) 1–12.
[13] A. Xu, L. Shi, T.S. Zhao, Lattice Boltzmann simulation of shear viscosity of suspensions containing porous particles, Int. J. Heat Mass Transf. 116 (2018) 969–976.
[14] D.D. Joseph, L.N. Tao, The effect of permeability on the slow motion of a porous sphere in a viscous liquid, Z. Angew. Math. Mech. 44 (1964) 361–364.
[15] S. Bhattacharyya, S. Dhinakaran, A. Khalili, Fluid motion around and through a porous cylinder, Chem. Eng. Sci. 61 (2006) 4451–4461.
[16] S. Shahsavari, B.L. Wardle, G.H. McKinley, Interception efficiency in two-dimensional flow past confined porous cylinders, Chem. Eng. Sci. 116 (2014) 752–762.
[17] H. Masoud, H.A. Stone, M.J. Shelley, On the rotation of porous ellipsoids in simple shear flows, J. Fluid Mech. 733 (2013) 733 R6–5 – 733 R6-11.
[18] C.G. Li, M. Ye, Z.M. Liu, On the rotation of a circular porous particle in 2D simple shear flow with fluid inertia, J. Fluid Mech. 808 (2016) [R3-1 – R3-13].
[19] L. Wang, L.P. Wang, Z.L. Guo, J.C. Mi, Volume-averaged macroscopic equation for fluid flow in moving porous media, Int. J. Heat Mass Transf. 82 (2015) 357–368.
[20] S. Tao, Z.L. Guo, L.P. Wang, Numerical study on the sedimentation of single and multiple slippery particles in a Newtonian fluid, Powder Technol. 315 (2017) 126–138.
[21] Z.G. Feng, E.E. Michaelides, The immersed boundary-lattice Boltzmann method for solving fluid–particles interaction problems, J. Comput. Phys. 195 (2004) 602–628.
[22] J.C. Ladd, Numerical simulations of particulate suspensions via a discretized Boltzmann equation. Part 2. Numerical results, J. Fluid Mech. 271 (1994) 311–339.
[23] Z.L. Guo, T.S. Zhao, Lattice Boltzmann model for incompressible flows through porous media, Phys. Rev. E 66 (1994) (2002) 311–339 036304-1-9. 271.
[24] H.B. Li, X.Y. Lu, H.P. Fang, Y.H. Qian, Force evaluations in lattice Boltzmann simulations with moving boundaries in two dimensions, Phys. Rev. E 70 (2004) 026701–1-9.
[25] R.W. Mei, D.Z. Yu, S. Wei, Force evaluation in the lattice Boltzmann method involving curved geometry, Phys. Rev. E 65 (2002) 041203–1-14.
[26] C.K. Aidun, Y. Lu, E.J. Ding, Direct analysis of particulate suspensions with inertia using the discrete Boltzmann equation, J. Fluid Mech. 373 (1998) 287–311.
[27] Q.S. Zou, X.Y. He, On pressure and velocity boundary conditions for the lattice Boltzmann BGK model, Phys. Fluids 9 (1997) 1591–1598.
[28] E.J. Ding, C.K. Aidun, The dynamics and scaling law for particles suspended in shear flow with inertia, J. Fluid Mech. 423 (2000) 317–344.